IRSTI 30.17.51

[1*]Ye. Belyayev, [2]A. Naimanova, [1]A. Kaltayev, [3]S. Jayaraj

[1]al-Farabi Kazakh National University, Almaty, Kazakhstan
[2]Institute of Mathematics and Mathematical Modelling, Ministry of Education and Science, Almaty, Kazakhstan
[3]Department of Mechanical Engineering, National Institute of Technology Calicut-673601, Kerala, India
*e-mail: yerzhan.belyayev@gmail.com

Numerical study of supersonic turbulent free shear layer mixing and combustion

Abstract. Numerical study of two-dimensional supersonic hydrogen-air mixing and combustion in free shear layer is performed. The system of Favre-Averaged Naveir-Stokes equations for multispecies reacting flow is solved using ENO scheme of third-order in accuracy. The k-ε two-equation turbulence models with compressibility correction are applied to calculate the eddy viscosity coefficient. In order to produce the roll-up and pairing of vortex rings, an unsteady boundary condition is applied at the inlet plane. At the outflow, the non-reflecting boundary condition is taken. The influence of different Mach numbers on the formation of vorticity structures and shear layer growth rate are studied. The obtained results are compared with available experimental data and the numerical results of other authors. For the description of reaction pathways of hydrogen, a seven species chemical reaction model by Jachimowski is adopted. The influence of Mach numbers on turbulent mixture and combustion is reported.
Key words: supersonic shear flow, mixing layer, hydrogen combustion, ENO-scheme, turbulence model, seven chemical reactions mechanism

Introduction

Compressible mixing layer is an important flow in extensive engineering applications. In particular, the shear layer configuration is a simple and yet fundamental to understand how fuel flow will mix and combust with supersonic oxidizer flow in SCRAM jet engines combustion chambers of hypersonic vehicles. As is well known the main objectives of investigating the physical processes in combustion chamber of these engines is aimed to maximize thrust by enhancing the fuel-air mixing and combustion.

It is necessary to take into account the influence of gas-dynamical structure, turbulence effects and chemical reactions for understanding physical structure of fuel-air mixture combustion in numerical model. Studying combustion in shear layer requires accurate predictions of mixing and combustion efficiency to which special attention should be paid to simulation the unsteady behavior of mixing layer roll-up and vortex formation. The gas-dynamical structure of mixing between two parallel super-subsonic flows has been comprehensively studied by many investigators. Nowadays, there are a large number of works on experimental [1-9], analytical [10-11] and numerical [12-27] study of this problem in the view of above physical effects as separately as with including all of them. Experimental efforts investigating the roll of large scale structures and growth mechanisms in compressible mixing layer have been done in sufficient details by researchers [1-6]. There are a great deal of researches devoted to the turbulence problem and influence of turbulence quantities on the mixing and vorticity formation [7-9].

The behavior of shear layers of perfect gases have been entirely realized in mathematical models, but the practical design of supersonic ramjet (scramjet) engines requires the shear layer growth enhancements for multispecies gases. Successful numerical models of such flows with the detail flow physics represent a difficult problem. Therefore the investigators studied some physical phenomena

 Printed in Kazakhstan

separately or proposed the numerical method, which are important for solution of this complex system. In [12, 15-16] have been modeled the free shear layer flowfield structures using the system of compressible Euler equations. For example, in [12] have been numerically studied the supersonic-subsonic free shear layer applying high order WENO scheme to the system of 2D axisymmetric Euler equations and numerical turbulence model taken as a SGS model. During numerical experiment revealed that at high-convective Mach number turbulence mixing rates reduces and vortex roll-up and pairing suppresses. In [13-14, 17] have been performed numerical experiment based on the system of Navier-Stokes equations for monatomic (air) gas to study the growth of instabilities in supersonic free shear layers. Xiao-Tian Shi et al. [17] conducted numerical simulations of compressible mixing layers based on discontinuous Galerkin method with inflow perturbation for prediction of the flowfield structures obtained in experiments. Numerical experiments of influence of unsteady inflow perturbations on the mixing in supersonic free shear layers on the basis of second and fourth order MacCormack scheme have been performed by authors [13-14]. Their studies revealed that normal velocity perturbation is more efficient than streamwise and spanwise. To date rarely performed the numerical investigation of growth of instabilities in shear layer using unsteady disturbances for multispecies gas mixture. In these works have accurately predicted the gas-dynamical structure of shear layers by advanced numerical methods without chemical reactions terms.

The mathematical model and numerical method of solution of supersonic combustion in shear layer flow has been performed for laminar [18-24] and turbulent [25-27] flows. In these works the basic efforts is directed on analysis of influence different effects such as inlet swirl, initial temperature, velocity and pressure ratios on ignition time delay. The detail chemical reaction mechanism during calculation have been adopted in [21, 25-26], while in [18-19, 23] reduced reaction mechanisms. For example, the numerical study of ignition in supersonic turbulent hydrogen-air mixing layer including detail chemical kinetics and advection upstream splitting method ($AUSM^+$) have performed in [25-26]. In this study illustrates that the swirl used in the fuel and oxidizer flows decreases the ignition time delay significantly by enhancing the swirl angle [25-26]. Numerically investigation of the ignition and combustion of hydrogen-air and ethylene-air mixture in supersonic shear flow configuration on the base of fourth-order accurate in space and second-order accurate in time MacCormak-like scheme with compact difference operators and automatic reduction procedure chemical kinetics, for various Mach numbers and temperatures have been made in [18-19]. In these investigations with the simulation of reacting shear layer were insufficiently paid attention to the vortical nature of mixing layer. Up to date there are few works on numerical study of unsteady combustion in supersonic shear layer.

In the present study, the third order essentially non-oscillatory (ENO) finite difference scheme is adopted to solve the system of Favre-averaged Navier-Stokes equations with chemical kinetics terms to supersonic planar shear layer. The k-ε two-equation turbulence model with compressibility correction is used to predict the turbulence characteristics. To verify the mathematical model and numerical algorithm obtained results compared with experimental study of Samimy and Elliot [8-9] for supersonic-subsonic free shear layer. Simulation of the flame propagation with combustion products formation is performed including the seven reaction and seven component Jachimowski's kinetics mechanism. The effect of flows Mach number on turbulent mixture and combustion of hydrogen-air flow is reported. For more information, see [36] and references therein.

The inflow physical parameters profile across the non-premixed hydrogen (fuel) and air stream at the splitter plate leading edge is assumed to vary smoothly according to a hyperbolic-tangent function (Fig. 1).

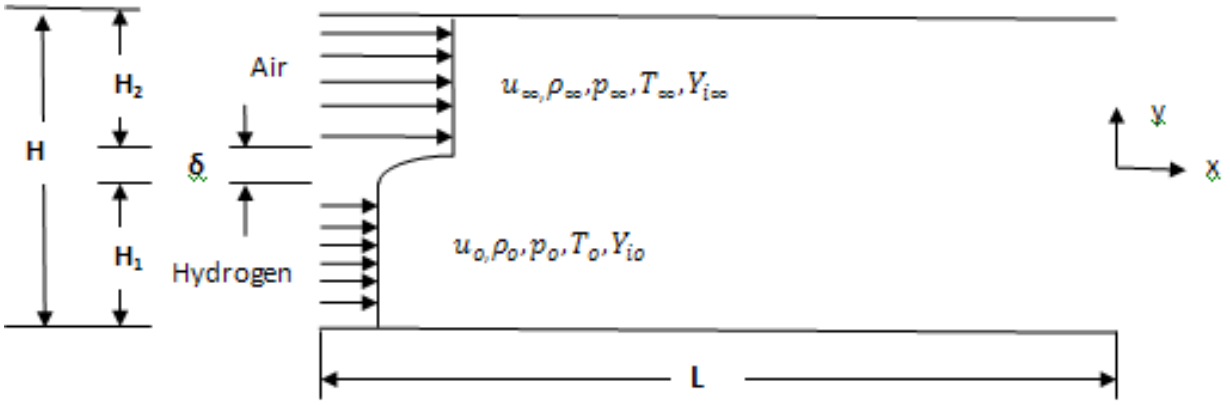

Figure 1 – An illustration of the flow configuration

Mathematical model

The two-dimensional Favre-averaged Navier-Stokes equations for multi-species flow with chemical reactions is:

$$\frac{\partial \vec{U}}{\partial t} + \frac{\partial (\vec{E} - \vec{E}_v)}{\partial x} + \frac{\partial (\vec{F} - \vec{F}_v)}{\partial z} = 0, \qquad (1)$$

where the vector of the dependent variables and the vector fluxes are given as

$$\vec{U} = \begin{pmatrix} \rho \\ \rho u \\ \rho w \\ E_t \\ \rho Y_k \\ \rho k \\ \rho \varepsilon \end{pmatrix}, \quad \vec{E} = \begin{pmatrix} \rho u \\ \rho u^2 + p \\ \rho uw \\ (E_t + p)u \\ \rho u Y_k \\ \rho uk \\ \rho u\varepsilon \end{pmatrix}, \quad \vec{F} = \begin{pmatrix} \rho w \\ \rho uw \\ \rho w^2 + p \\ (E_t + p)w \\ \rho w Y_k \\ \rho wk \\ \rho w\varepsilon \end{pmatrix},$$

$$\vec{E}_v = \left(0, \tau_{xx}, \tau_{xz}, u\tau_{xx} + w\tau_{xz} - q_x, J_{kx}, \frac{1}{\mathrm{Re}}\left(\mu_l + \frac{\mu_t}{\sigma_k}\right)\frac{\partial k}{\partial x}, \frac{1}{\mathrm{Re}}\left(\mu_l + \frac{\mu_t}{\sigma_\varepsilon}\right)\frac{\partial \varepsilon}{\partial \mathrm{x}}\right)^T,$$

$$\vec{F}_v = \left(0, \tau_{xz}, \tau_{zz}, u\tau_{xz} + w\tau_{zz} - q_z, J_{kz}, \frac{1}{\mathrm{Re}}\left(\mu_l + \frac{\mu_t}{\sigma_k}\right)\frac{\partial k}{\partial z}, \frac{1}{\mathrm{Re}}\left(\mu_l + \frac{\mu_t}{\sigma_\varepsilon}\right)\frac{\partial \varepsilon}{\partial z}\right)^T,$$

$$\vec{W} = \left(0,0,0,0,0, \left[P_k - \rho\varepsilon\left(1 + \alpha M_t^2\right) + D\right], \left[C_{\varepsilon 1} P_k \varepsilon / k - C_{\varepsilon 2} f_{\varepsilon 2} \rho \varepsilon^2 / k\right]\right)^T$$

Here, the viscous stresses, thermal conduction, and diffusion flux of species are:

$$\tau_{xx} = \frac{1}{\mathrm{Re}}\left(\mu_l + \frac{\mu_t}{\sigma_k}\right)\left(2u_x - \frac{2}{3}(u_x + w_z)\right);$$

$$\tau_{zz} = \frac{1}{\mathrm{Re}}\left(\mu_l + \frac{\mu_t}{\sigma_k}\right)\left(2w_z - \frac{2}{3}(u_x + w_z)\right);$$

$$\tau_{xz} = \tau_{zx} = \frac{1}{\mathrm{Re}}\left(\mu_l + \frac{\mu_t}{\sigma_k}\right)(u_z + w_x);$$

$$q_x = \frac{1}{\Pr \mathrm{Re}}\left(\mu_l + \frac{\mu_t}{\sigma_k}\right)\frac{\partial T}{\partial x} + \frac{1}{\gamma_\infty M_\infty^2}\sum_{k=1}^{N} h_k J_{xk};$$

$$q_z = \frac{1}{\Pr \mathrm{Re}}\left(\mu_l + \frac{\mu_t}{\sigma_k}\right)\frac{\partial T}{\partial z} + \frac{1}{\gamma_\infty M_\infty^2}\sum_{k=1}^{N} h_k J_{zk};$$

$$J_{kx} = -\frac{1}{Sc\,\mathrm{Re}}\left(\mu_l + \frac{\mu_t}{\sigma_k}\right)\frac{\partial Y_k}{\partial x},$$

$$J_{kz} = -\frac{1}{Sc\,\mathrm{Re}}\left(\mu_l + \frac{\mu_t}{\sigma_k}\right)\frac{\partial Y_k}{\partial z}.$$

Parameters of the turbulence are:

$$P_k = \tau_{txx}\frac{\partial u}{\partial x} + \tau_{txz}\frac{\partial u}{\partial z} + \tau_{tzx}\frac{\partial w}{\partial x} + \tau_{tzz}\frac{\partial w}{\partial z};$$

$$\tau_{txx} = \frac{\mu_t}{\mathrm{Re}}\left(2\frac{\partial u}{\partial x} - \frac{2}{3}\left(\frac{\partial u}{\partial x} + \frac{\partial w}{\partial z}\right)\right);$$

$$\tau_{txz} = \frac{\mu_t}{\mathrm{Re}}\left(\frac{\partial u}{\partial z} + \frac{\partial w}{\partial x}\right);$$

$$\tau_{tzz} = \frac{\mu_t}{\mathrm{Re}}\left(2\frac{\partial w}{\partial z} - \frac{2}{3}\left(\frac{\partial u}{\partial x} + \frac{\partial w}{\partial z}\right)\right);$$

$$M_t^2 = 2 \cdot M_\infty^2 \cdot k / T;$$

$$f_{\varepsilon 2} = 1 - 0.3 \cdot \exp\left(-\mathrm{Re}_t^2\right), \quad \mathrm{Re}_t = \mathrm{Re}\left(\frac{\rho k^2}{\mu_l \varepsilon}\right);$$

$$C_{\varepsilon 1} = 1.44; C_{\varepsilon 2} = 1.92; \sigma_k = 1.0; \sigma_\varepsilon = 1.3,$$

where k, ε – turbulent kinetic energy, rate of dissipation of turbulent kinetic energy. P_k – is turbulence production term, M_t – is the turbulence Mach number.

Y_k – is the mass fraction of k^{th} species, $\dot{\omega}_k$ – rate of mass production of species, $k = 1 \ldots N$, with N – number a components in a gas mixture. The thermal equation for multi-species gas is:

$$p = \frac{\rho T}{\gamma_\infty M_\infty^2 W}, \quad W = \left(\sum_{k=1}^{N}\frac{Y_k}{W_k}\right)^{-1}, \quad \sum_{k=1}^{N} Y_k = 1 \qquad (2)$$

where W_k is the molecular weight of the species.

The equation for a total energy is given by

$$E_t = \frac{\rho h}{\gamma_\infty M_\infty^2} - p + \frac{1}{2}\rho\left(u^2 + w^2\right) \qquad (3)$$

The enthalpy of the gas mixture is calculated according to $h = \sum_{k=1}^{N} Y_k h_k$, with specific enthalpy of k^{th} species evaluated suing $h_k = h_k^0 + \int_{T_0}^{T} c_{pk} dT$.

The specific heat at constant pressure for each component c_{pk} is:

$$c_{pk} = C_{pk} / W, \; C_{pk} = \sum_{i=1}^{5} \overline{a}_{ki} T^{(i-1)}, \; \overline{a}_{jk} = a_{jk} T_\infty^{\,j-1}$$

where the molar specific heat C_{pk} is given in terms of the fourth degree polynomial with respect to temperature, consistent with the JANAF Thermochemical Tables [28].

The system of the equations (1) is written in the conservative, dimensionless form. The air flow parameters are $\rho_\infty, u_\infty, w_\infty, T_\infty, h_\infty, W_\infty, R_\infty$, hydrogen jet parameters are $\rho_0, u_0, w_0, T_0, h_0, W_0, R_0$. The governing parameters are the air flow parameters, the pressure and total energy are normalized by $\rho_\infty u_\infty^2$, the enthalpy by $R_0 T_\infty / W_\infty$, the molar specific heat by R_0 and the spatial distances by the thickness of the splitter plate δ.

The coefficient of viscosity is represented in the form of the sum of μ_l – molecular viscosity and μ_t – turbulent viscosity: $\mu = \mu_l + \mu_t$, where μ_t is defined according to k-ε model with compressibility correction. The mixture averaged molecular viscosity is evaluated using from Wilke's formula.

The chemical reactions of hydrogen H_2 with air are described using Jachimowski's seven species model used in the NASA SPARK code [28]. This model includes the following seven species: $H_2, O_2, H_2O, OH, H, O, N_2$.

Initial and boundary conditions

At the entrance:

$u_1 = M_0\sqrt{\frac{\gamma_0 R_0 T_0}{W_0}}$, $w_1 = 0$, $p_1 = p_0$, $T_1 = T_0$, $Y_{k1} = Y_{k0}$, $k = k_0$, $\varepsilon = \varepsilon_0$ at $x = 0$, $0 \leqslant z < \mathrm{H}_1$.

$u_2 = M_\infty\sqrt{\frac{\gamma_\infty R_0 T_\infty}{W_\infty}}$, $w_2 = 0$, $p_2 = p_\infty$, $T_2 = T_\infty$, $Y_{k2} = Y_{k\infty}$, $k = k_\infty$, $\varepsilon = \varepsilon_\infty$ at $x=0$, $H_1 + \delta \leqslant z \leqslant H_2$.

In the region of $H_1 \leqslant z \leqslant H_1 + \delta$ all physical variables are varied smoothly from hydrogen (fuel) flow to air flow using a hyperbolic-tangent function of any variable φ, so the inflow profiles are defined by

$$\phi(z) = 0.5(\phi_2 + \phi_1) + 0.5(\phi_2 - \phi_1)\tanh(0.5z/\theta)$$

at $x = 0$, $0 \le z \le H$.

where $\phi = (u, v, p, T, Y_k, k, \varepsilon)$, θ - is the momentum thickness. The pressure is assumed to be uniform across the shear layer. On the lower and upper boundary the condition of symmetry are imposed. At the outflow, the non-reflecting boundary condition is used [29].

In order to produce the roll-up and pairing of vortex rings, an unsteady boundary condition is also applied at the inlet plane, i.e.

$$u = u(z) + A\Delta U Gaussian\,(z)\cos(\omega t)$$

$$w = \Delta w_{factor}\, A\Delta U Gaussian\,(z)\sin(\omega t)$$

$$Gaussian(z) = \exp(-z^2/2\sigma^2),$$

where $u(z)$ _ velocity profile at the entrance corresponding to hyperbolic-tangent function. The unsteady part of the condition is about 0.2-0.3 percent of the Favre-averaged velocity. $\Delta U = (u_\infty - u_0)$ – the difference of two stream velocities which measures the strength of shearing. $Gaussian\,(z)$ – is a Gaussian function which has a peak value of unity at z=0 and the $\pm 2\sigma$ width was matched to the vorticity layer thickness at the entrance. Coefficient A is the disturbance amplitude which is defined from the $A \cdot \Delta U$, where this product was specified to be 0.2-0.3 percent of the higher inflow speed. The Δw_{factor} was set at 0.7 (70%) of $A \cdot \Delta U$ based on [16]. The $\omega = 2\pi\left(\frac{\left(\sqrt{\frac{\gamma_0 R_0 T_0}{W_0}} + \sqrt{\frac{\gamma_\infty R_\infty T_\infty}{W_\infty}}\right)/2}{2\delta_w}\right)$ is the frequency of perturbation. $\delta_w = \frac{(u_\infty - u_0)}{(\partial u/\partial z)_{\max}}$ – is the vorticity thickness.

Method of solution

To take into account the flow in the shear (at the entrance) and mixing layer, i.e., in regions of high gradients, more accurately, we refine the grid in the longitudinal and transverse directions by the transformations

$$\frac{\partial \tilde{U}}{\partial t} + \frac{\partial \tilde{E}}{\partial \xi} + \frac{\partial \tilde{F}}{\partial \eta} = \frac{\partial \tilde{E}_{v2}}{\partial \xi} + \frac{\partial \tilde{E}_{vm}}{\partial \xi} + \frac{\partial \tilde{F}_{v2}}{\partial \eta} + \frac{\partial \tilde{F}_{vm}}{\partial \eta}, \qquad (4)$$

where $\tilde{U} = \vec{U}/J$, $\tilde{E} = \xi_x \vec{E}/J$, $\tilde{F} = \eta_z \vec{F}/J$, $\tilde{E}_{v2} = \xi_x \vec{E}_{v2}/J$, $\tilde{E}_{vm} = \xi_x \vec{E}_{vm}/J$, $\tilde{F}_{v2} = \eta_z \vec{F}_{v2}/J$, $\tilde{F}_{vm} = \eta_z \vec{F}_{vm}/J$, and $J = \partial(\xi,\eta)/\partial(x,z)$ is the Jacobian of mapping.

System (4) linearized with respect to the vector U in form:

$$\tilde{U}^{n+1} + \Delta t\left(\frac{\partial \tilde{E}^{n+1}}{\partial \xi} + \frac{\partial \tilde{F}^{n+1}}{\partial \eta} - \frac{\partial \tilde{E}_{vm}^{n+1}}{\partial \xi} - \frac{\partial \tilde{E}_{v2}^{n+1}}{\partial \xi} - \frac{\partial \tilde{F}_{vm}^{n+1}}{\partial \eta} - \frac{\partial \tilde{F}_{v2}^{n+1}}{\partial \eta}\right) = \tilde{U}^n + O(\Delta t^2). \qquad (5)$$

Here,

$$\tilde{E}^{n+1} \approx A_\xi^n \tilde{U}^{n+1},\ \tilde{F}^{n+1} \approx B_\eta^n \tilde{U}^{n+1}, \qquad (6)$$

$A_\xi = \xi_x A$, $B_\eta = \eta_z B$, $A = \partial\vec{E}/\partial\vec{U}$, $B = \partial\vec{F}/\partial\vec{U}$ – are the Jacobian matrices [32-33].

The terms containing the second derivatives are presented as sums of two vectors:

$$\tilde{E}_{v2}^{n+1} = \tilde{E}_{v21}^{n+1} + \tilde{E}_{v22}^{n},\quad \tilde{F}_{v2}^{n+1} = \tilde{F}_{v21}^{n+1} + \tilde{F}_{v22}^{n}, \qquad (7)$$

where the vectors $\tilde{E}_{v21}^{n+1}$, $\tilde{F}_{v21}^{n+1}$ are written in the following form:

$$\widetilde{E}_{v21}^{\mathrm{n}+1}=\frac{\mu_t\xi_x}{\mathrm{Re}\,J}\left[0,\frac{4}{3}\frac{\partial}{\partial\xi}\left(\frac{u\rho}{\rho}\right)^{n+1},\frac{\partial}{\partial\xi}\left(\frac{w\rho}{\rho}\right)^{n+1},\frac{\gamma}{\mathrm{Pr}}\frac{\partial}{\partial\xi}\left(\frac{E_t}{\rho}\right)^{n+1}\right]^T,$$

$$\widetilde{F}_{v21}^{\mathrm{n}+1}=\frac{\mu_t\eta_z}{\mathrm{Re}\,J}\left[0,\frac{\partial}{\partial\eta}\left(\frac{u\rho}{\rho}\right)^{n+1},\frac{4}{3}\frac{\partial}{\partial\eta}\left(\frac{w\rho}{\rho}\right)^{n+1},\frac{\gamma}{\mathrm{Pr}}\frac{\partial}{\partial\eta}\left(\frac{E_t}{\rho}\right)^{n+1}\right]^T,$$

and the vectors $\widetilde{E}_{v12}^{\mathrm{n}}$, $\widetilde{F}_{v22}^{n}$ contain the remaining dissipative functions of the form:

$$\widetilde{E}_{v12}^{\mathrm{n}}=\frac{\xi_x^2}{\mathrm{Re}\,J}\left[0,0,0,\left[\left(\mu-\frac{\gamma\mu}{\mathrm{Pr}}\right)\left(w\frac{\partial w}{\partial\xi}\right)+\left(\frac{4}{3}\mu-\frac{\gamma\mu}{\mathrm{Pr}}\right)u\frac{\partial u}{\partial\xi}\right]^n\right]^T,$$

$$\widetilde{F}_{v22}^{\mathrm{n}}=\frac{\eta_z^2}{\mathrm{Re}\,J}\left[0,0,0,\left[\left(\mu-\frac{\gamma\mu}{\mathrm{Pr}}\right)\left(u\frac{\partial u}{\partial\eta}\right)+\left(\frac{4}{3}\mu-\frac{\gamma\mu}{\mathrm{Pr}}\right)w\frac{\partial w}{\partial\eta}\right]^n\right]^T,$$

$$\tilde{E}_{vm}=\frac{\xi_x\mu_t}{ReJ}\left[0,-\frac{2}{3}\left(\eta_z\frac{\partial w}{\partial\eta}+\zeta_y\frac{\partial v}{\partial\zeta}\right),\eta_z\frac{\partial u}{\partial\eta},-\frac{2}{3}\left(\zeta_y u\frac{\partial v}{\partial\zeta}+\eta_z u\frac{\partial w}{\partial\eta}\right)+\left(\eta_z w\frac{\partial u}{\partial\eta}+\zeta_y v\frac{\partial u}{\partial\zeta}\right)\right],.$$

$$\tilde{F}_{vm}=\frac{\eta_z\mu_t}{ReJ}\left[0,\eta_z\frac{\partial w}{\partial\eta},-\frac{2}{3}\left(\xi_x\frac{\partial u}{\partial\xi}+\zeta_y\frac{\partial w}{\partial\zeta}\right),\left(\xi_x u\frac{\partial w}{\partial\xi}+\zeta_y u\frac{\partial w}{\partial\zeta}\right)-\frac{2}{3}\left(\xi_x w\frac{\partial u}{\partial\xi}+\zeta_y w\frac{\partial v}{\partial\zeta}\right)\right].$$

According to a principle of construction ENO scheme [30-31] the system (5) for integration on time is formally represented as:

$$\begin{aligned}&\Delta\tilde{U}^{n+1}+\\&+\Delta t\left[\left(\hat{A}^{+}+\hat{A}^{-}\right)\frac{\partial\vec{E}^{m}}{\partial\xi}+\left(\hat{B}^{+}+\hat{B}^{-}\right)\frac{\partial\vec{F}^{m}}{\partial\eta}-\right.\\&\left.-\left[\frac{\partial(\tilde{E}_{v2}{}^{n+1}+\tilde{E}_{vm}{}^{n})}{\partial\xi}-\frac{\partial(\tilde{F}_{v2}{}^{n+1}+\tilde{F}_{vm}{}^{n})}{\partial\eta}\right]\right]=\\&=O\left(\tfrac{1}{2}\Delta t^2\right)\end{aligned}\qquad(8)$$

Here $\vec{E}^{m}$, $\vec{F}^{m}$ is called the modified flux vector. It consists from the original flux vector ($\tilde{E}$, $\tilde{F}$ and additional terms of third-order accuracy $\vec{E}_\xi,\vec{D}_\xi$, $\vec{E}_\eta,\vec{D}_\eta$) :

$$\vec{E}^{m}=\tilde{E}^{n+1}+(\vec{E}_\xi+\vec{D}_\xi)^n\ ,\qquad(9)$$

modified flux $\vec{F}^{m}$ is written similarly and $A^{+}+A^{-}=I$, $A^{\pm}=A^{\pm}A^{-1}$, $B^{\pm}=B^{\pm}B^{-1}$, I - unity matrix.

Applying factorization to (8), we obtain two one-dimensional operators, which are resolved by matrix sweep:

Step 1:

$$\left[I + \Delta t \left\{ (A^{+}_{i-1/2}\Delta_{-} A^{n}_{\xi} + A^{-}_{i+1/2}\Delta_{+} A^{n}_{\xi}) + \Delta \frac{\mu_t \xi_x^2}{\mathrm{Re}\, J} \Delta \frac{1}{U_1^n} \right\} \right] \mathrm{U}^{*} = RHS^{n}_{\xi} + RHS^{n}_{\eta}$$

Step 2:

$$\left[I + \Delta t \left\{ (B^{+}_{j-1/2}\Delta_{-} B^{n}_{\eta} + B^{-}_{j+1/2}\Delta_{+} B^{n}_{\eta}) + \Delta \frac{\mu_t \eta_z^2}{\mathrm{Re}\, J} \Delta \frac{1}{U_1^n} \right\} \right] \tilde{\mathrm{U}}^{n+1} = \mathrm{U}^{*}, \tag{10}$$

$$RHS^{n}_{\xi} = A^{-}_{i+1/2j}\left[\left(\vec{E}_{\xi} + \vec{D}_{\xi}\right)_{i+1j} - \left(\vec{E}_{\xi} + \vec{D}_{\xi}\right)_{ij} \right]^{n} + A^{+}_{i-1/2j}\left[\left(\vec{E}_{\xi} + \vec{D}_{\xi}\right)_{ij} - \left(\vec{E}_{\xi} + \vec{D}_{\xi}\right)_{i-1j} \right]^{n},$$

$$A^{-}_{i+1/2j}\left[\left(\vec{E}_{\zeta} + \vec{D}_{\zeta}\right)_{ij} \right]^{n} = \left(\boldsymbol{minmod}\left(\overline{E}_{\xi i+1/2j}\ \overline{E}_{\xi i-1/2j}\right) + \right.$$

$$\left. + \begin{cases} \dot{\boldsymbol{m}}\left(\Delta_{-} D_{\xi i+1/2j},\ \Delta_{+} D_{\xi i+1/2j}\right) & \text{if} \quad \left|\Delta_{-}\tilde{U}_{ij}\right| > \left|\Delta_{+}\tilde{U}_{ij}\right| \\ \dot{\boldsymbol{m}}\left(\Delta_{-} \overline{D}_{\xi i-1/2j},\ \Delta_{+} \overline{D}_{\xi i-1/2j}\right) & \text{if} \quad \left|\Delta_{-}\tilde{U}_{ij}\right| \le \left|\Delta_{+}\tilde{U}_{ij}\right| \end{cases} \right),$$

$$A^{+}_{i-1/2j}\left[\left(\vec{E}_{\xi} + \vec{D}_{\xi}\right)_{ij} \right]^{n} = R\,\Lambda^{+} R^{-1}_{i-1/2j} \left[\left(\boldsymbol{minmod}\left(\overline{E}_{\xi i+1/2j}\ \overline{E}_{\xi i-1/2j}\right) - \right.\right.$$

$$\left.\left. - \begin{cases} \dot{\boldsymbol{m}}\left(\Delta_{-} D_{\xi i-1/2j},\ \Delta_{+} D_{\xi i-1/2j}\right) & \text{if} \quad \left|\Delta_{-}\tilde{U}_{ij}\right| \le \left|\Delta_{+}\tilde{U}_{ij}\right| \\ \dot{\boldsymbol{m}}\left(\Delta_{-} \overline{D}_{\xi i-1/2j},\ \Delta_{+} \overline{D}_{\xi i-1/2j}\right) & \text{if} \quad \left|\Delta_{-}\tilde{U}_{ij}\right| \le \left|\Delta_{+}\tilde{U}_{ij}\right| \end{cases} \right],$$

$$\overline{E}_{\xi i\pm 1/2j} = \left(R\, sign\,(\Lambda) R^{-1}\right)_{i\pm 1/2j} \frac{1}{2}\left[I - \frac{\Delta t}{\Delta \xi} \left(R\,|\Lambda|\,R^{-1}\right)_{i\pm 1/2} \right] \Delta_{\pm} \tilde{E}_{ij},$$

$$\overline{D}_{\xi i\pm 1/2j} = \left(R\, sign\,(\Lambda) R^{-1}\right)_{i\pm 1/2j} \frac{1}{6}\left[\frac{\Delta t^2}{\Delta \xi^2} \left(R\,|\Lambda|\,R^{-1}\right)^{2}_{\pm} - I \right] \Delta_{\pm} \tilde{E}_{ij},$$

$$D_{\xi i\pm 1/2j} = \overline{E}_{\xi i\pm 1/2j} + \overline{D}_{\xi i\pm 1/2j},$$

where:

$$\boldsymbol{minmod}\,(a,b) = \begin{cases} s \cdot min\left(|a|,|b|\right) & \text{if} \quad sign(a) = sign(b) = s \\ 0 & \text{other} \end{cases},$$

$$\dot{\boldsymbol{m}}(a,b) = \begin{cases} a & \text{if} \quad |a| \le |b| \\ b & \text{if} \quad |a| > |b| \end{cases}.$$

The second term $RHS^n{}_\eta$ is written similarly.

In approximation of derivatives in convective and diffusion terms, we use second-order central-difference operators.

The numerical solution of the system (5) is calculated in two steps. The first determines the dynamic parameters and second determines the mass species.

Then it is necessary to define Jacobian matrix which in a case of the thermally perfect gas represents difficult task. This problem is connected with the explicit representation of pressure through the unknown parameters. Here pressure is determined by introducing an effective adiabatic parameter of the gas mixture [34].

$$\bar{\gamma} = \frac{h_{sm}}{e_{sm}}\ , \qquad (11)$$

where $h_{sm} = \sum_{i=1}^{N} Y_i \int_{T_0}^{T} c_{p_i} dT$, $e_{sm} = \sum_{i=1}^{N} Y_i \int_{T_0}^{T} c_{v_i} dT$ – is the enthalpy and internal energy of the mixture minus the heat and energy of formation; $T_0 = 293\ K$ - is the standard temperature of formation, which allows to write an expression for the pressure

$$p = (\bar{\gamma} - 1)\left[E_t - \frac{1}{2}\rho\left(u^2 + w^2\right) - \rho\frac{h_0}{\gamma_\infty M_\infty^2} \right] + \frac{\rho T_0}{M_\infty^2 W}.$$

The temperature is found from the Newton-Raphson iteration [32-33, 35].

The equations for species are solved by the scalar sweep, where in the first-step convection and diffusion terms are included and calculated using ENO scheme [30-31]. In the second-step, the matrix equation with terms ($\dot{w}_k = W_k \dot{\omega}_k$) is solved implicitly. These source terms $\dot{W}_k$ are linearized by expansion in a Taylor series,

$$\dot{W}_k^{n+1} = \dot{W}_k^n + \gamma\left(\frac{\partial \dot{W}_k}{\partial Y_m}\Delta Y_m + \frac{\partial \dot{W}_k}{\partial T}\Delta T + \frac{\partial \dot{W}_k}{\partial \rho}\Delta\rho \right)$$

Results and discussion

The parameters of coordinate transformation have the form:

$$\xi(x) = H\left[(\beta+1) - (\beta-1)\left(\frac{\beta+1}{\beta-1}\right)^{1-\frac{x}{L}} \right] \Bigg/ \left[\left(\frac{\beta+1}{\beta-1}\right)^{1-\frac{x}{L}} + 1 \right], \quad \eta(z) = K + \frac{1}{\tau} arsh\left[\left(\frac{z}{z_c} - 1\right) sh(\tau K) \right],$$

$$K = \frac{1}{2\tau} \ln\left[\left(1 + (e^\tau - 1)\frac{z_c}{H}\right) \Bigg/ \left(1 - (e^\tau - 1)\frac{z_c}{H}\right) \right],$$

β, τ are refinement factors (β>1 and τ>1), L – is the length of the computational domain in the generalized coordinates, and z_c – is the point with respect to which grid refinement is performed.

Previously the shear layer problem for monatomic (air) gas has been tested by the following parameters: M_0 = 0.51, T_0 = 285.07 K, P_0 = 56088.91 Pa, M_∞ = 1.8, T_∞ = 176.58 K, P_∞ = 54648.65 Pa. The computational grid is 526x201. The channel height and length were 8 cm and 50 cm, respectively. The splitter plate thickness is 0.3175 cm, and at the trailing edge is 0.05 cm. The initial momentum thickness $\theta = \int_{-\infty}^{+\infty} \left(\frac{\rho}{\rho_\infty} u^* \left(1 - u^*\right) dz \right)$ is 0.05 cm. The geometrical parameters above are taken from experimental work of Samimy and Elliot [8-9].

Experiment was conducted in tunnel, present calculation performed for planar channel to estimate the behavior of turbulence quantities. Figures 2-4 shows (M_c – 0.51) the comparison of the calculated distributions of longitudinal (axial) mean velocity, variation of the momentum (θ) and vorticity (δ_w) thicknesses, and turbulence quantities with the

experimental data [8-9]. The non-dimensional variables $u^* = \frac{(u-u_0)}{(u_\infty - u_0)}$, $z^* = \frac{(z-z_c)}{\delta_w}$, $\theta = \int_{-\infty}^{+\infty}\left(\frac{\rho}{\rho_\infty}u^*(1-u^*)dz\right)$, $\delta_w = \frac{(u_\infty - u_0)}{(\partial u/\partial z)_{\max}}$ are defined as in the experiments [8-9]. Figure 2 indicates that the shear layer growth in terms of momentum and vorticity thickness is predicted reasonably accurate by the present algorithm, as compared to experimental data.

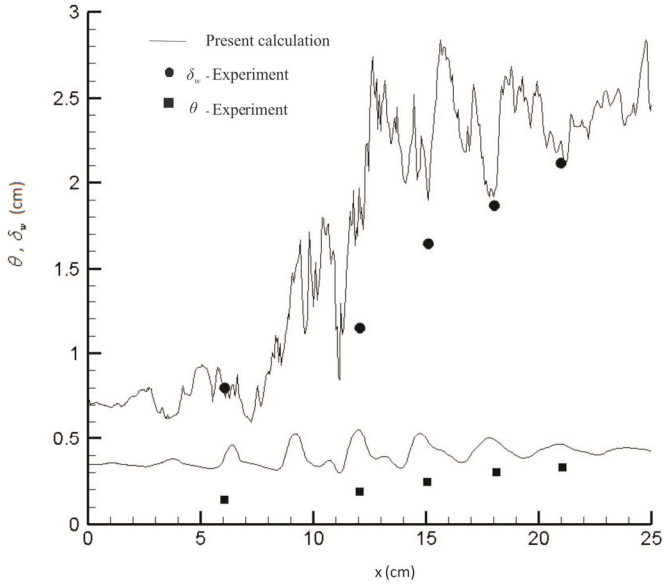

Figure 2 – Comparison of present calculation with experimental data by the growth of momentum and vorticity thickness

The comparison of calculated transverse distribution of the normalized streamwise mean velocity at five longitudinal positions with experimental measurements as shown in Figure 3 suggest that in the fully developed region for x≥12 cm the mean flow is self-similar.

Further comparison of the calculated results with experimental data are shown for the development of the Reynolds stress $-\overline{u'v'}/(u_\infty - u_o)^2$ in Figures 4 and streamwise turbulence intensity $\sqrt{2/3k}/(u_\infty - u_o)$ in Figure 5. The contribution of transverse velocity fluctuating component to turbulent kinetic energy was neglected. It is visible from figures that the calculated turbulence quantities are distorted at x≥15 cm, which shows that the turbulence similarity is achieved further downstream than the mean flow similarity. The preliminary test shown that the mean and turbulence quantities are in a good agreement with experimental data.

In the sequel the shear layer problem has been numerically studied for multi-component gas mixture with the following parameters without chemical reactions and turbulence model: M_0 = 2.3, T_0 = 400 *K*, P_0 = 101320 *Pa*, M_∞ = 4.0, T_∞ = 800 *K*, P_∞ = 101320 *Pa*. The computational grid is 526x201. The non-dimensional channel height and length were 100 and 367, respectively. According to [13-14] it was assumed that there is initial vorticity thickness ($\delta_w = \frac{(u_\infty - u_0)}{(\partial u/\partial z)_{\max}}$) at the inflow, δ_w = 1/15. Figure 6 shows the comparison of mixing layer growth by density a, c and vorticity b, d contours in two physical domain a-b 100x20 and c-d 367x100.

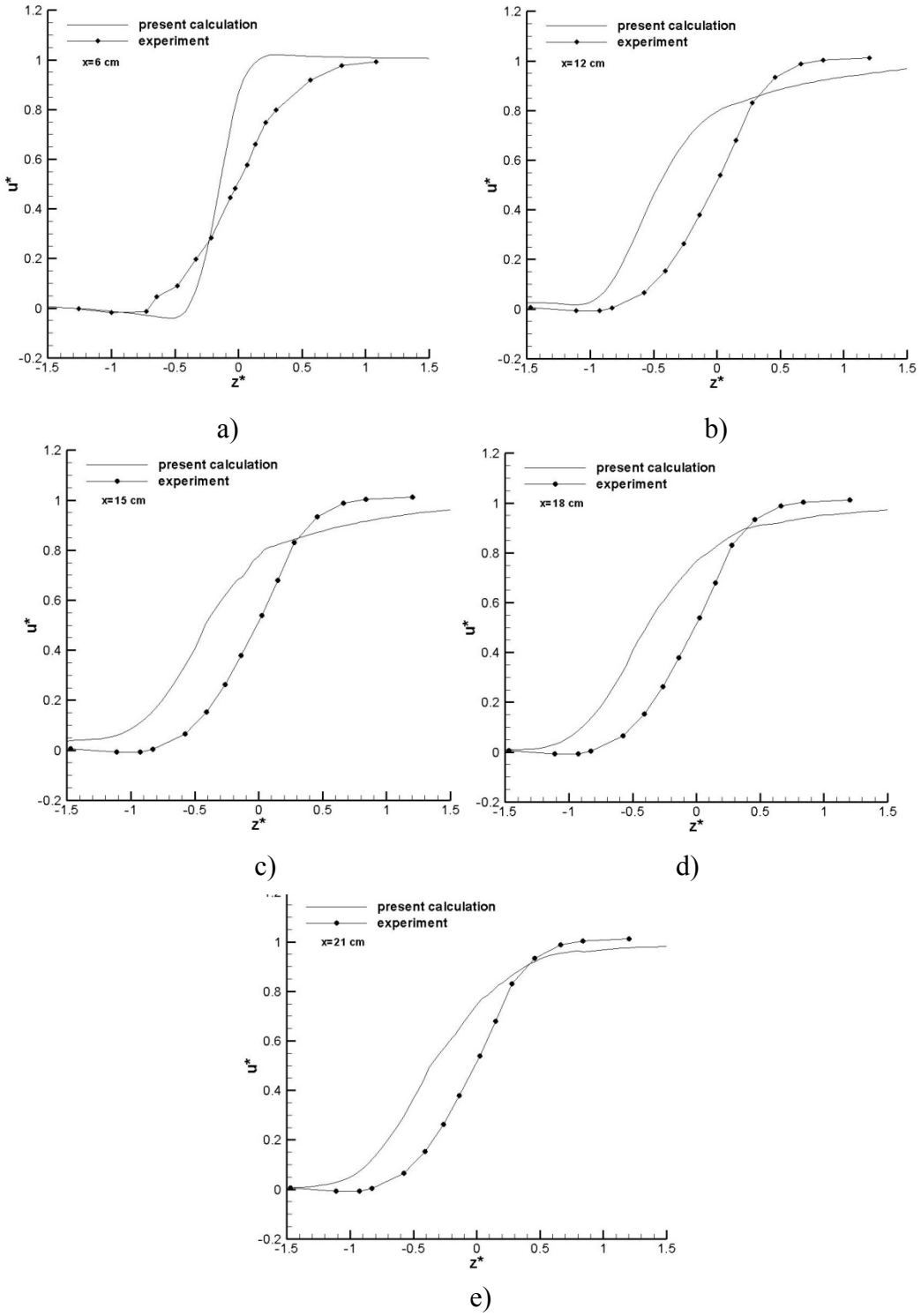

Figure 3 – Comparison of present calculation with experimental data
by longitudinal mean velocity profiles at five longitudinal positions in the shear layer
a) x=6, b) x=12, c) x=15, d) x=18, e) x=21 cm

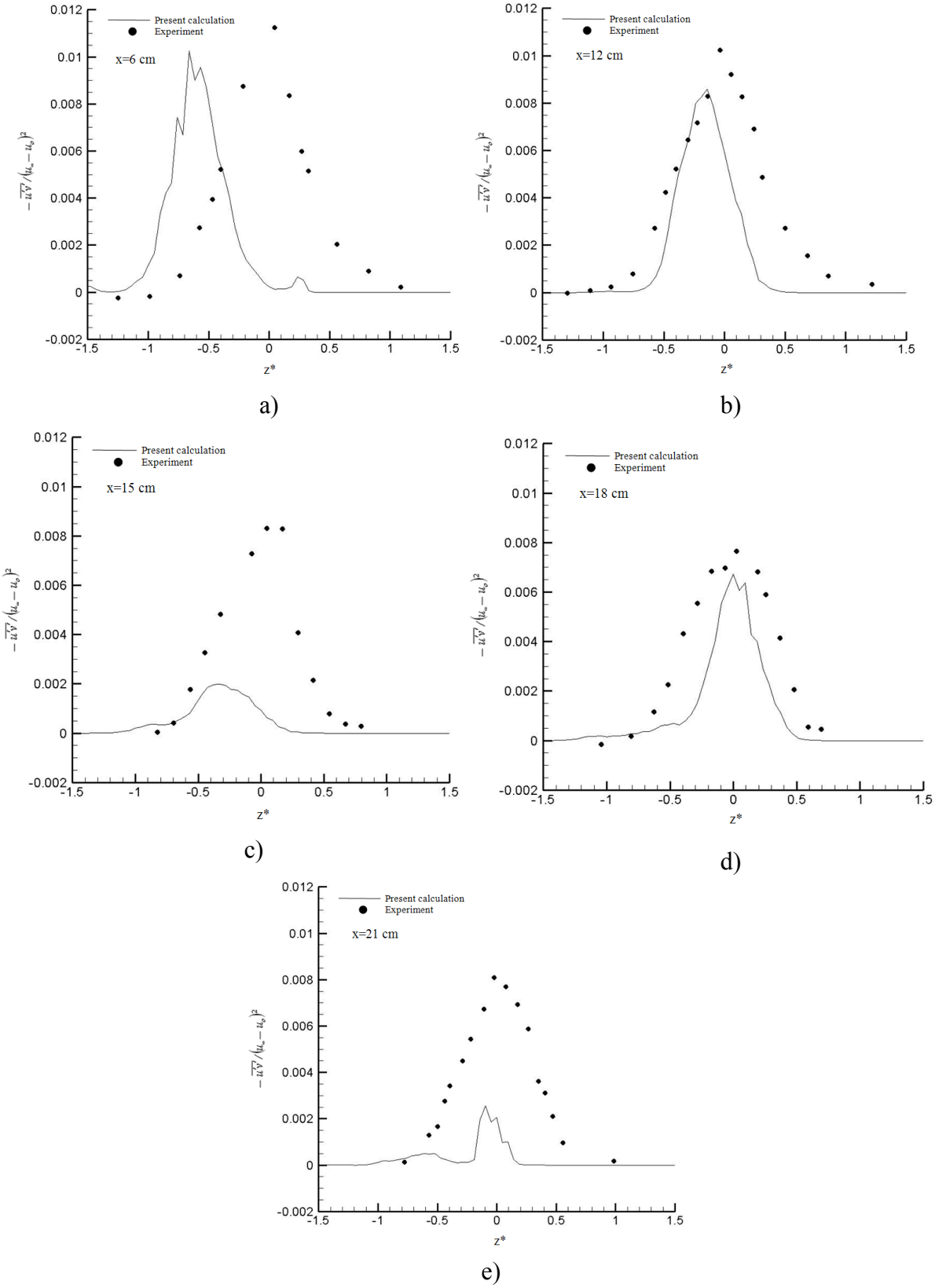

Figure 4 – Comparison of present calculation with experimental data by Reynolds stress at five longitudinal positions in the shear layer a) x=6, b) x=12, c) x=15, d) x=18, e) x=21 cm

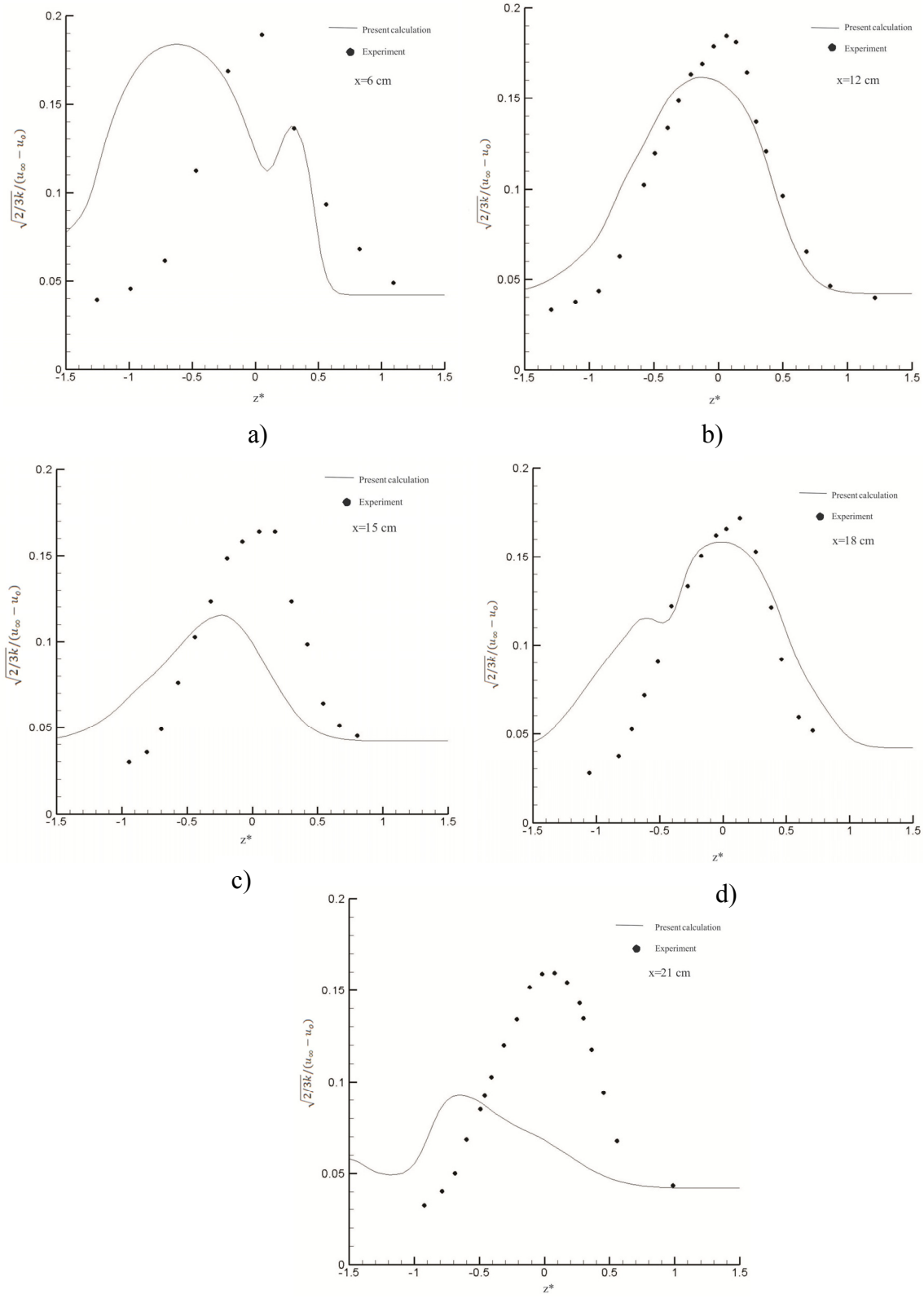

Figure 5 – Comparison of present calculation with experimental data by turbulent intensity at five longitudinal positions in the shear layer a) x=6, b) x=12, c) x=15, d) x=18, e) x=21 cm

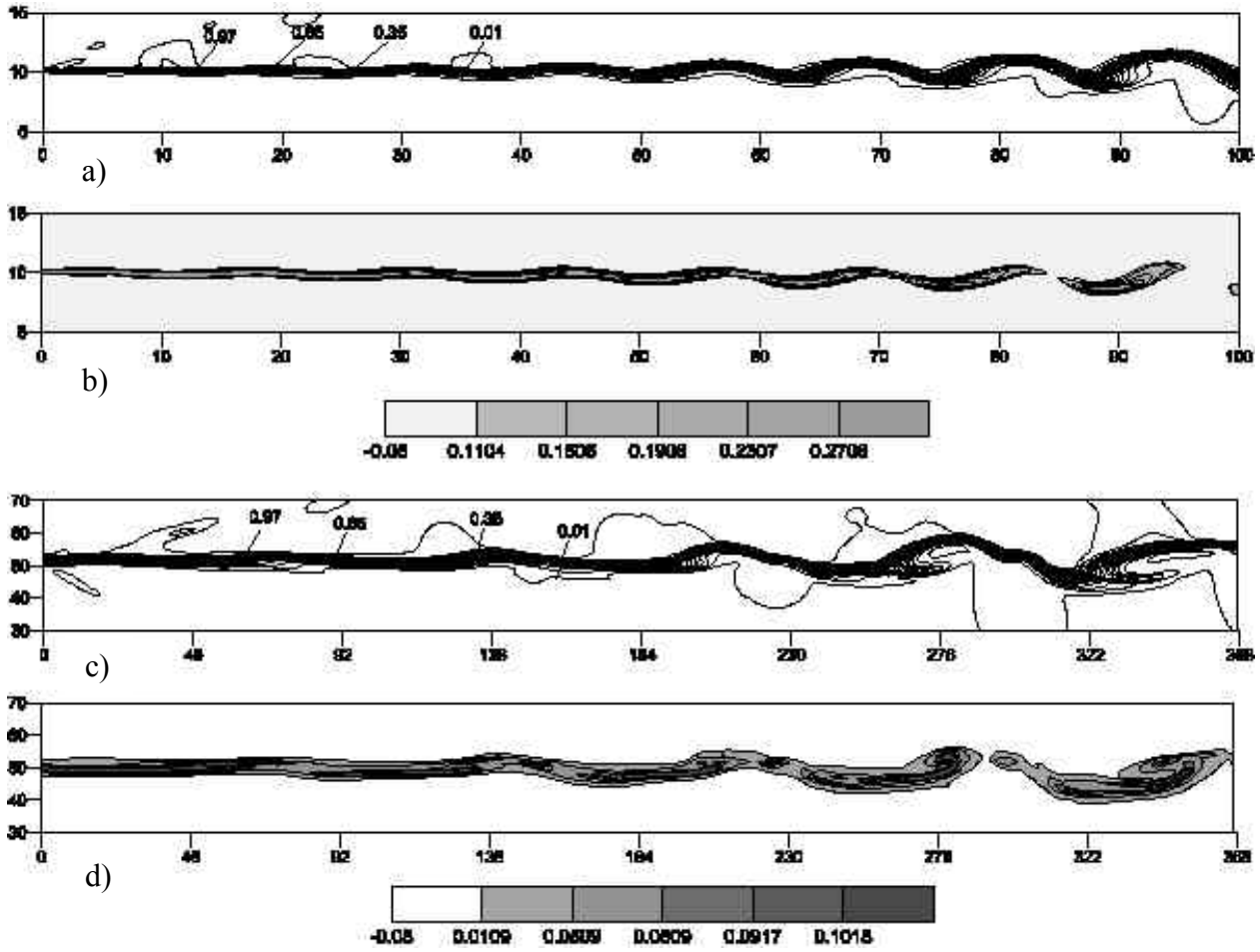

Figure 6 – Comparison of mixing layer growth
by density and vorticity contours in two physicaldomain
a-b) 100x20, c-d) 367x100

It visible from Figure 6 that in c, d the growth of the mixing layer is larger than in a, b. As the supersonic shear layer growth slower than subsonic, so to the formation of vortical structures and its growth in supersonic shear layer need longer domain (Figure 6-c-d). Figure 7 shows the comparison of vorticity contours obtained by present calculation and by authors [13-14]. In [13-14] studied the growth of instabilities in monatomic (air) gas flows, while in the present study considered the mixing layer growth in multi-component gas mixture. Present results indicate that in the case of multi-component gas the vortical structure has a growing character as it is shown in Figure 7-b.

Also, this example show the advantage of using high order ENO scheme in modeling of mixing process, formation and growing of vortical structures.

Combustion results

The free shear layer of hydrogen-air turbulent flows mixing and combustion are numerically studied. The simulations are performed in a rectangular domain of 4 cm in stream-wise direction and 1.5 cm in transverse direction. The splitter plate thickness is 0.1 cm, and at the trailing edge is 0.0045 cm. At the inflow plane, hydrogen enters from the lower half and air enters from the upper half. A 401x151 grid with stretching at the entrance and mixing layer was used. The hydrogen flow parameters are $M_0 = 1.4$ ($M_0 = 1.1$), $T_0 = 400$ K, $P_0 = 101320$ Pa, and air flow parameters are $M_\infty = 1.8$ ($M_\infty = 1.5$), $T_\infty = 1300$ K, $P_\infty = 101320$ Pa.

The Figure 8-a, c, d, f ($M_0 = 1.4$, $M_\infty = 1.8$) are illustrated the comparison of temperature fields

without and with chemical reactions for moments t=5.35 mks (Figure 8-a-c) and t =10.6 mks (Figure 8-d-f). The temperature for both cases is equal to 0.97 (1261 K) at t=5.35 mks. From figure follows mixing layer growth lead to an increase in the temperature and mixing intensity of fuel and oxidizer. It is evident from Figure 8-a, c the difference between results are negligible, consequently at the ignition stage the chemical reactions passes without significant heat generation. At the moment t=10.6 mks the temperature of the mixture increase till 1.1 (T=1430 K) due to chemical reaction, while in the non-reacting case the mixture temperature is 0.97.

For the description of reaction pathways of hydrogen, a seven species chemical reaction model by Jachimowski (see table 1 [31]) is taken.

The water vapor H_2O formation for the chemical reaction case at the ignition moment t=5.35 mks (Figure 8-b) and at the moment t=10.6 mks (Figure 8-e) are also illustrated.

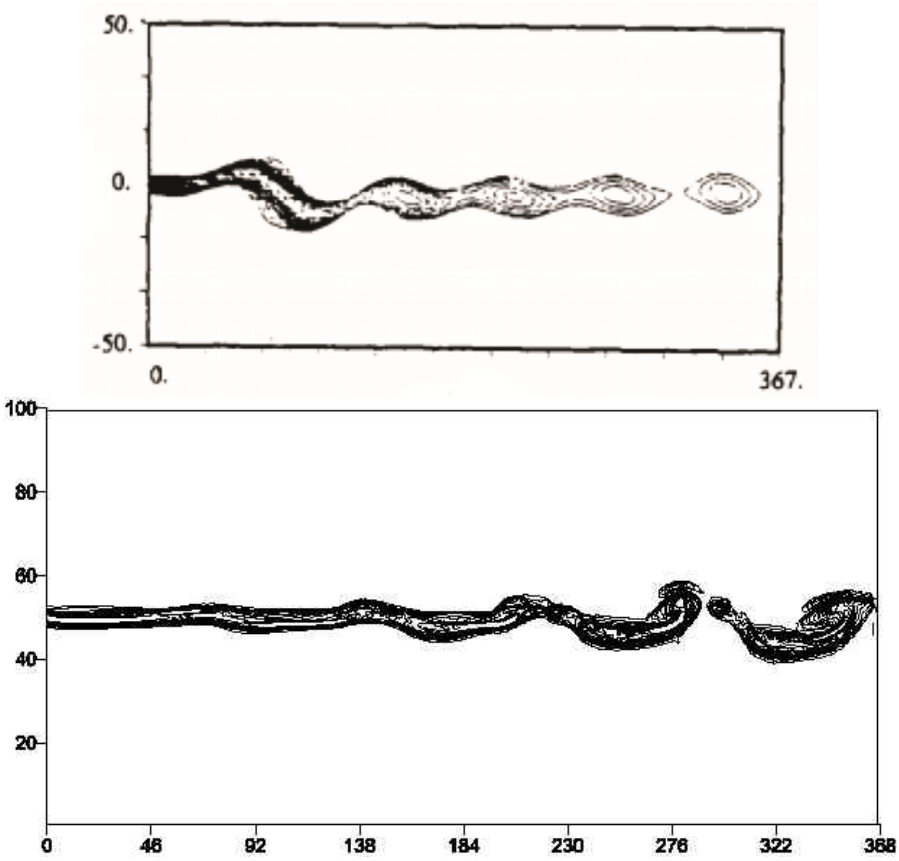

Figure 7 – Comparison of present calculation with numerical results [13-14] by vorticity contours
a) numerical results [13-14], b) present calculation

Table 1 – Jachimowski's reaction mechanism

Reaction number	Reaction	A_k (m^3/mole·s)	β_k	E_k/R
1	$H_2 + O_2 = OH + OH$	0.170E +14	0.0	24233
2	$H + O_2 = OH + O$	0.142E +15	0.0	8254
3	$OH + H_2 = H_2O + H$	0.316E +08	1.8	1525
4	$O + H_2 = OH + H$	0.207E +15	0.0	6920
5	$OH + OH = H_2O + O$	0.550E +14	0.0	3523
6	$H + OH + M = H_2O + M$	0.221E +23	-2.0	0
7	$H + H + M = H_2 + M$	0.653E +18	-1.0	0

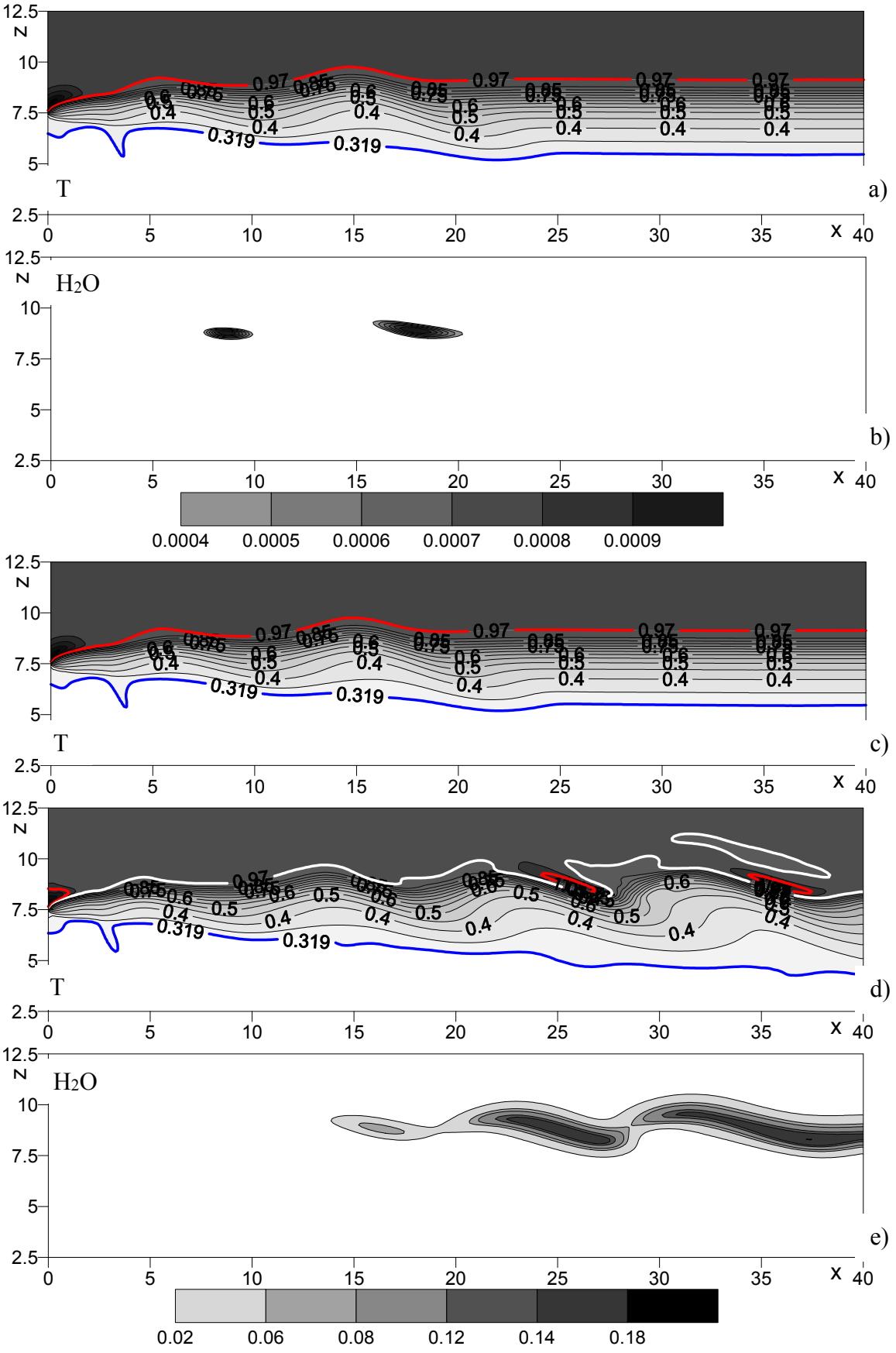
z
x
T
a)
H2O
b)
0.0004 0.0005 0.0006 0.0007 0.0008 0.0009
T
c)
T
d)
H2O
e)
0.02 0.06 0.08 0.12 0.14 0.18

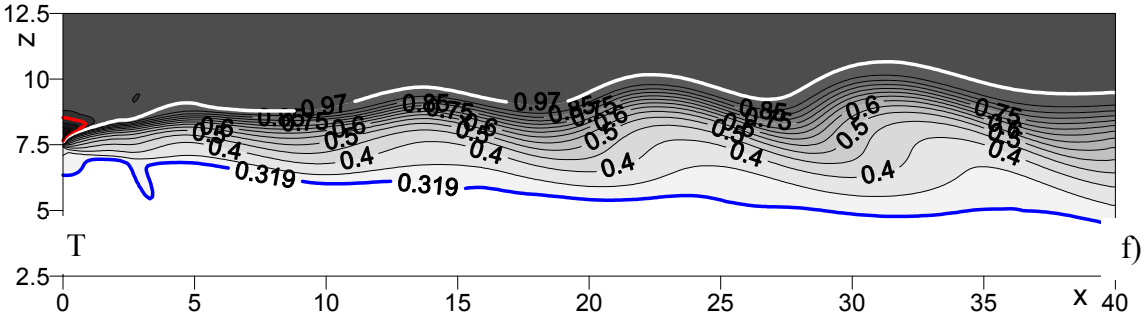

Figure 8 – The temperature field with a, c) and without b, d) chemical reactions
a-b) t=5.35, c-d) t=10.6 mks

Figure 9 shows the mass concentration contours of oxidant (Figure 9-a-b) and hydrogen (Figure 9-c-d) with combustion (Figure 9-b, d) and without it (Figure 9-a, c) at the moment t=10.6 mks. As can be seen from the figure as a result of combustion the oxidant O_2 field change significantly (Figure 9-b), while the hydrogen H_2 changes little (Figure 9-d). The isolines of the formation of combustion products such as water vapor (H_2O), hydroxyl radical (OH), hydrogen atom (H) and oxygen atom (O) concentrations and vorticity contours at various times are presented in Figures 10-13.

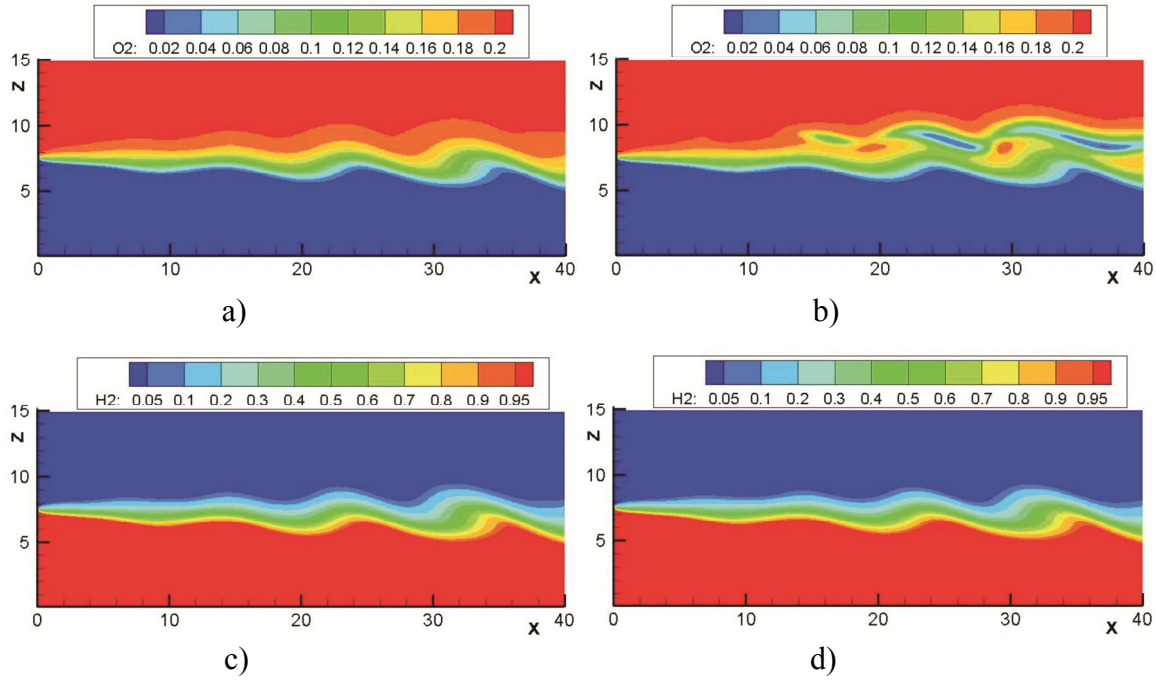

Figure 9 – Mass concentration contours of O_2 a-b) and H_2 c-d)

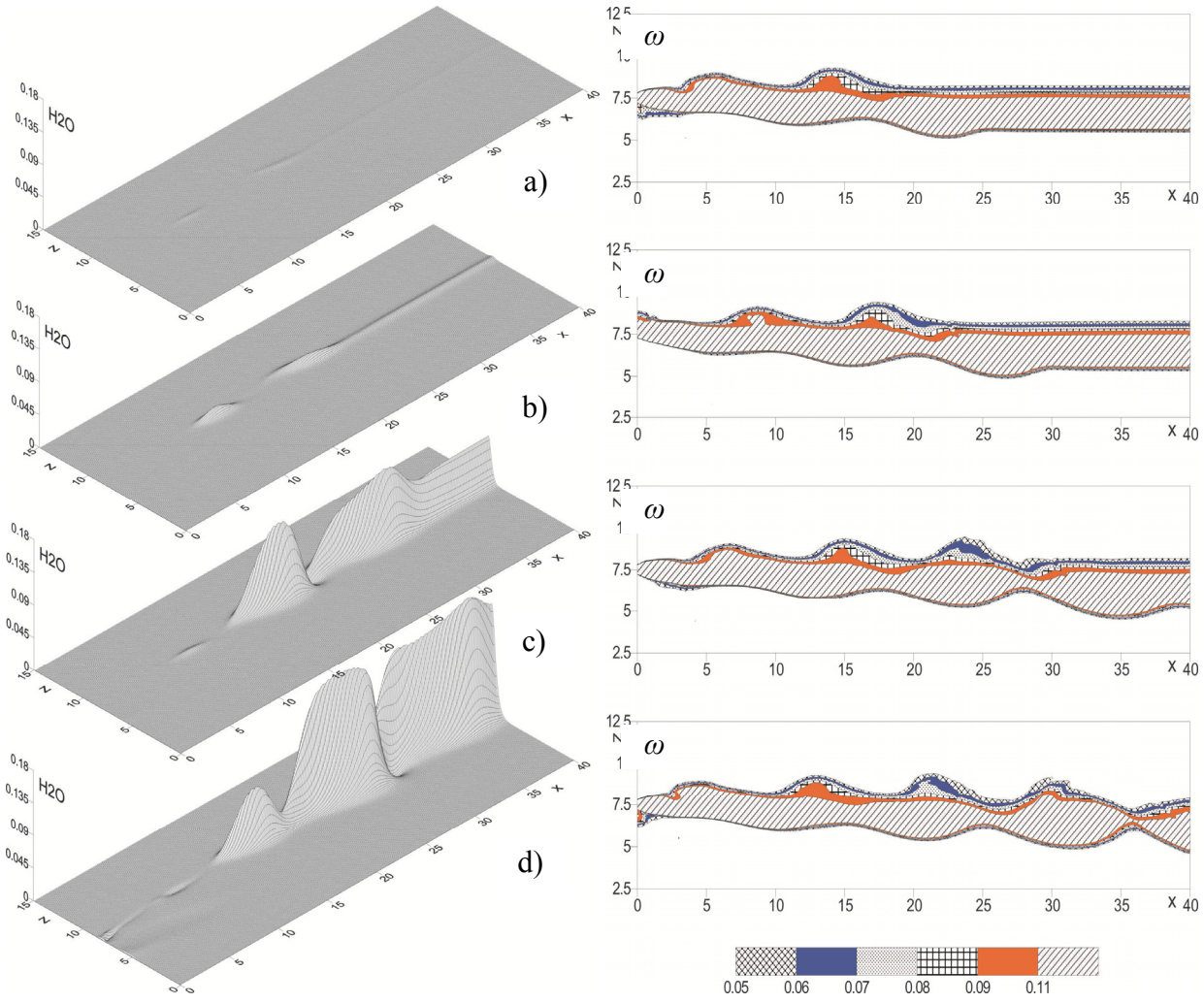

Figure 10 – The dynamic of water vapor concentration formation and vorticity contours at four times
a) t=5.35, b) t=6.4, c) t=8.5, d) t=10.6 mks

It is visible (Figure 10-a), initially combustion product H_2O is concentrated in the thin mixing layer at the moment t=5.35 mks. In this time the maximum of water vapor is of the order 10^{-4}, Figure 10-a. From the period of time t=5.35 up to t=6.4 mks (Figure 10-b) this value growth up to 10^{-3}. Obviously, it is the induction period which is period of accumulation of radicals and active centers, where there is also growth reaction rate.

The vorticity contours formed in the shear layer are illustrated in Figure 10-a-d (right, ω). In process of time the separation of vortical structure occurs Figure 10-b-d, thus with increasing of vorticity formation intensity (Figure 10-b-d, right) the separation of combustion zone concentrated in the upper region of vortices (Figure 10-b-d, left). The same behavior has products OH, H and O as it is illustrated in Figures 11-13-b-d, right with different induction period of formation. For example, the water vapor H_2O (Figure 10-a, left) and oxygen atom O (Figure 13-a) are formed earlier at t=5.35 mks than hydroxyl radical OH at t=5.7 mks (Figure 11-a) and hydrogen atom H at t=6.75 mks (Figure 12-a).

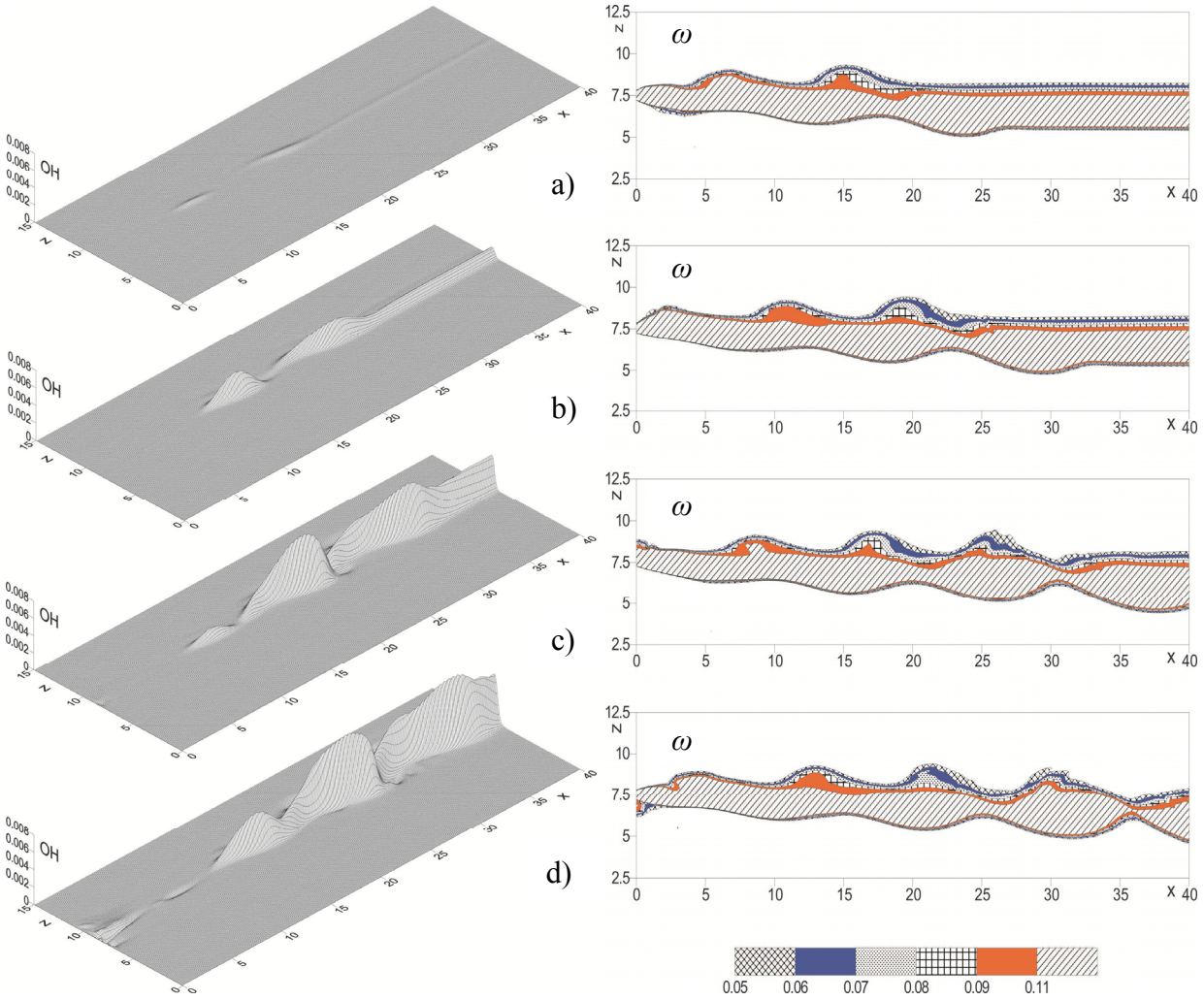

Figure 11 – The dynamic of hydroxyl radical concentration formation and vorticity contours at four times
a) t=5.7, b) t=7.1, c) t=9.2, d) t=10.6 mks

Numerical calculations performed with lower values of Mach numbers $M_0 = 1.1$, $M_\infty = 1.5$ are showed the presence of subsonic zones, which are visible from iso-Mach line contours in Figure 14-a. The minimum value of Mach number for $M_0 = 1.1$, $M_\infty = 1.5$ is 0.8, while for $M_0 = 1.4$, $M_\infty = 1.8$ this value is equal to 1.0. However, comparing with the higher Mach number case Figure 14-d the presence of subsonic zones does not have appreciable influence on the qualitative picture of combustion zone (Figure 14-c, f). Although, quantitatively this difference is more visible. For example, the maximum of water vapor and temperature are 0.16 and 1.1 (1430 K) for the case $M_0 = 1.4$, $M_\infty = 1.8$ whereas for other case maximum H2O is equal to 0.19 and temperature is 1.18 (T=1534 K). Therefore the occurrence of subsonic zones has insignificantly affects on combustion zone, whereas that the crucial aspect is the presence of vortical structures. The determinative factor in combustion stabilization and efficiency is the formation of vortices and their growth.

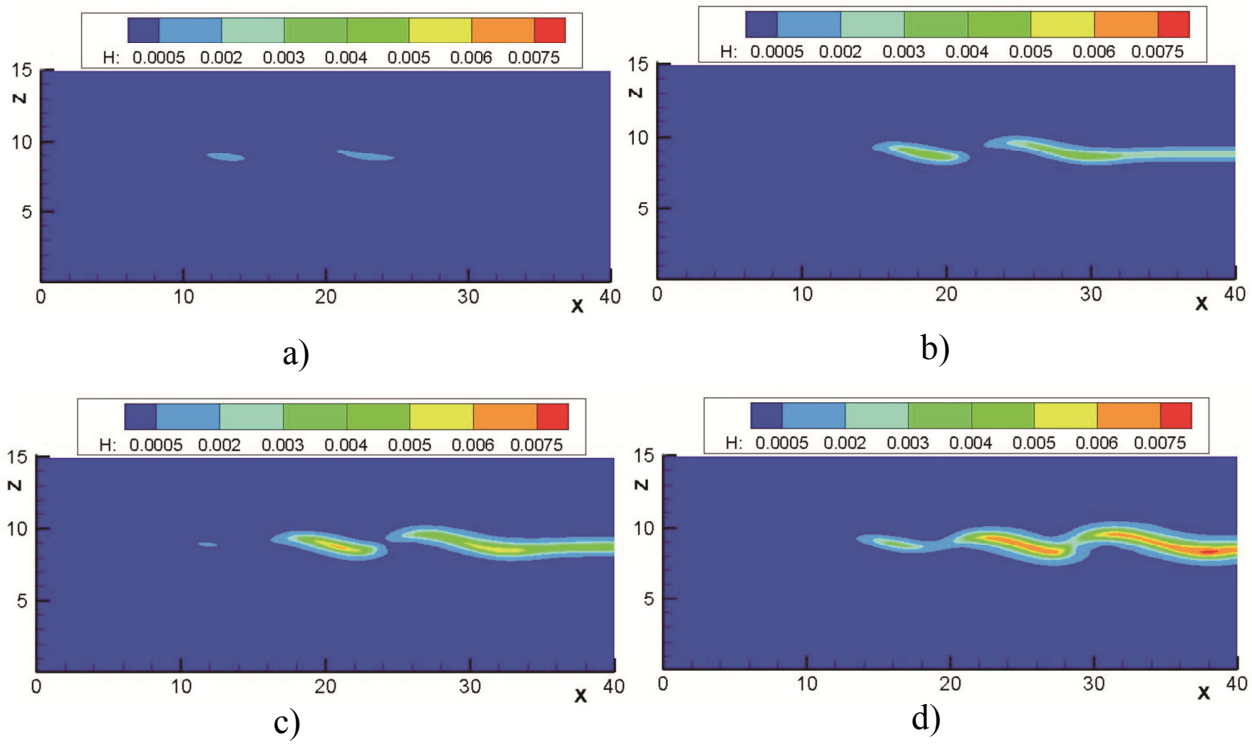

Figure 12 – The dynamic of hydrogen atom concentration formation at four times
a) t=6.75, b) t=8.5, c) t=9.2, d) t=10.6 mks

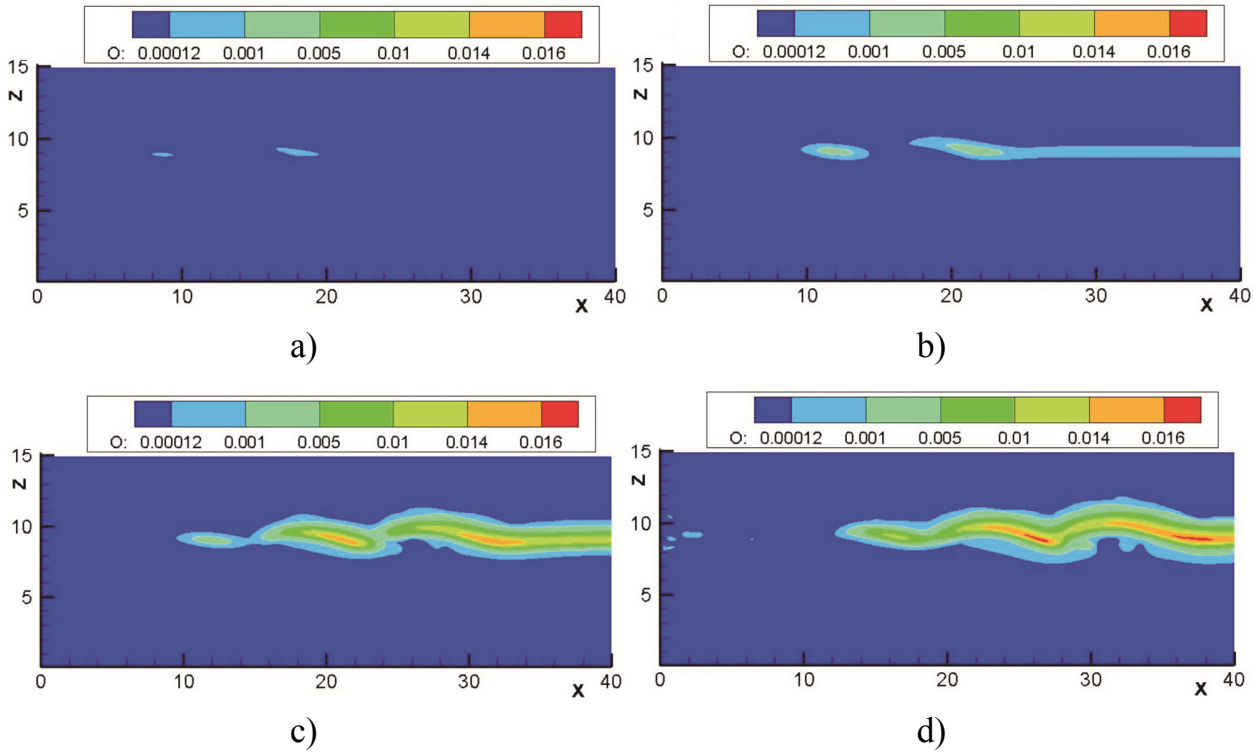

Figure 13 – The dynamic of hydrogen atom concentration formation at four times
a) t=5.35, b) t=6.4, c) t=9.2, d) t=10.6 mks

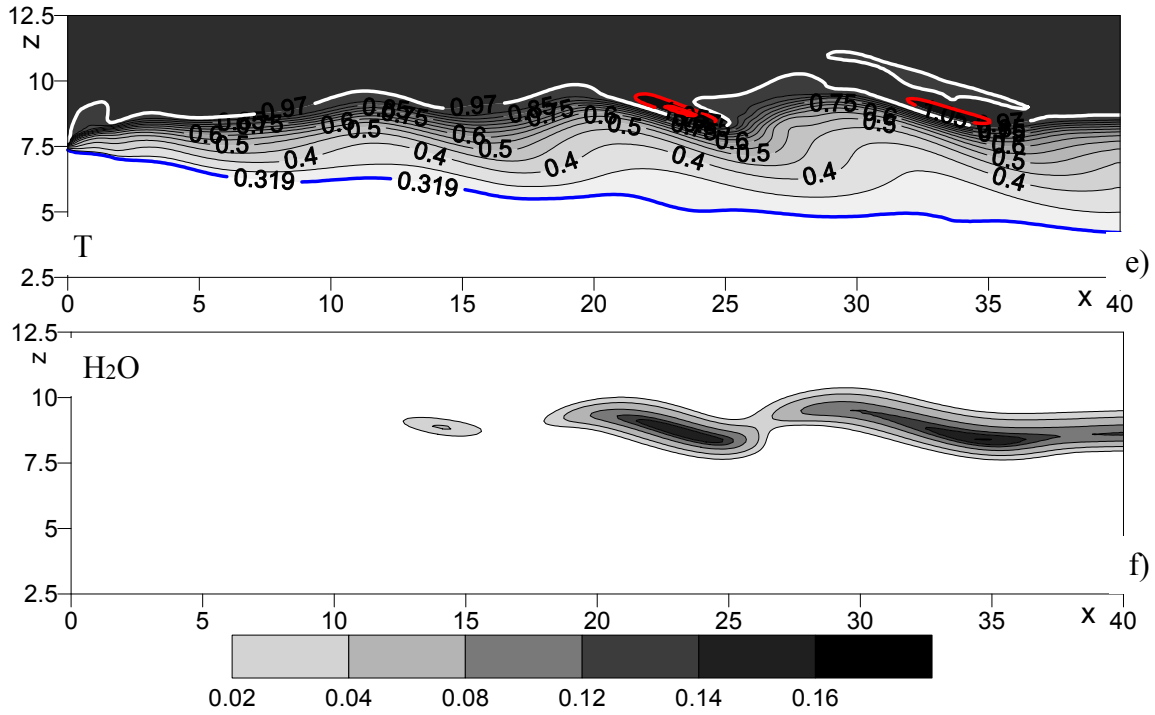

Figure 14 – The distribution of iso-Mach a, d), hydrogen b, e) and water vapor concentration c, f) contours
a-c) $M_0 = 1.1$, $M_\infty = 1.5$
d-f) $M_0 = 1.4$, $M_\infty = 1.8$

It should be noted the process of ignition represented in the Figure 15 are different for given cases. From isolines of water vapor concentration H_2O Figure 15-b, d are visible the ignition delay time is t=1.25 mks for result with smaller parameter, while for large Mach numbers are t=5.35 mks. The temperature in the ignition region for both cases Figure 15-a, c is equal to 0.97 (1261 K). As a identifier of the given mixture ignition it was taken the main product – water vapor H_2O with the value approximately 0.2 percent of initial oxidant fracture.

The combustion efficiency can be estimated from the overall chemical reaction of hydrogen oxidation. It appears from this reaction that for the 0.004 kg/mole hydrogen completely oxidation it is need 0.032 kg/mole oxygen. As a parameter characterized complete combustion it is taken the relation of the mass flow rates Q_{O2}/Q_{H2}, where $Q_{O2} = \int \rho_{O2} u_\infty dz$ and $Q_{H2} = \int \rho_{H2} u_0 dz$. This relation should be $Q_{O2}/Q_{H2} \geqslant 8$ to complete hydrogen combustion. Numerical experiment revealed that for the $M_0 = 1.4$, $M_\infty = 1.8$ at the exit plane x=4 cm this relation is equal to 18.7, which is pointing out that the hydrogen completely oxidize. The initial mass flow rates ratio at the entrance for this case $Q_{O2}/Q_{H2} = 14.8$, which indicate on the poor mixture. For Mach numbers $M_0 = 1.1$, $M_\infty = 1.5$ the initial mass flow rates ratio $Q_{O2}/Q_{H2} = 15.6$. At the exit plane x=4 cm combustion efficiency parameter is equal to 19.8. This comparison has been confirmed that subsonic zones have not strong affect on increasing the total residence time of fuel (hydrogen) in the combustion chamber. So the presence of isolated vortices and their growth downstream provides a better mixing of fuel, air and hot combustion products, which greatly stabilizes the combustion process.

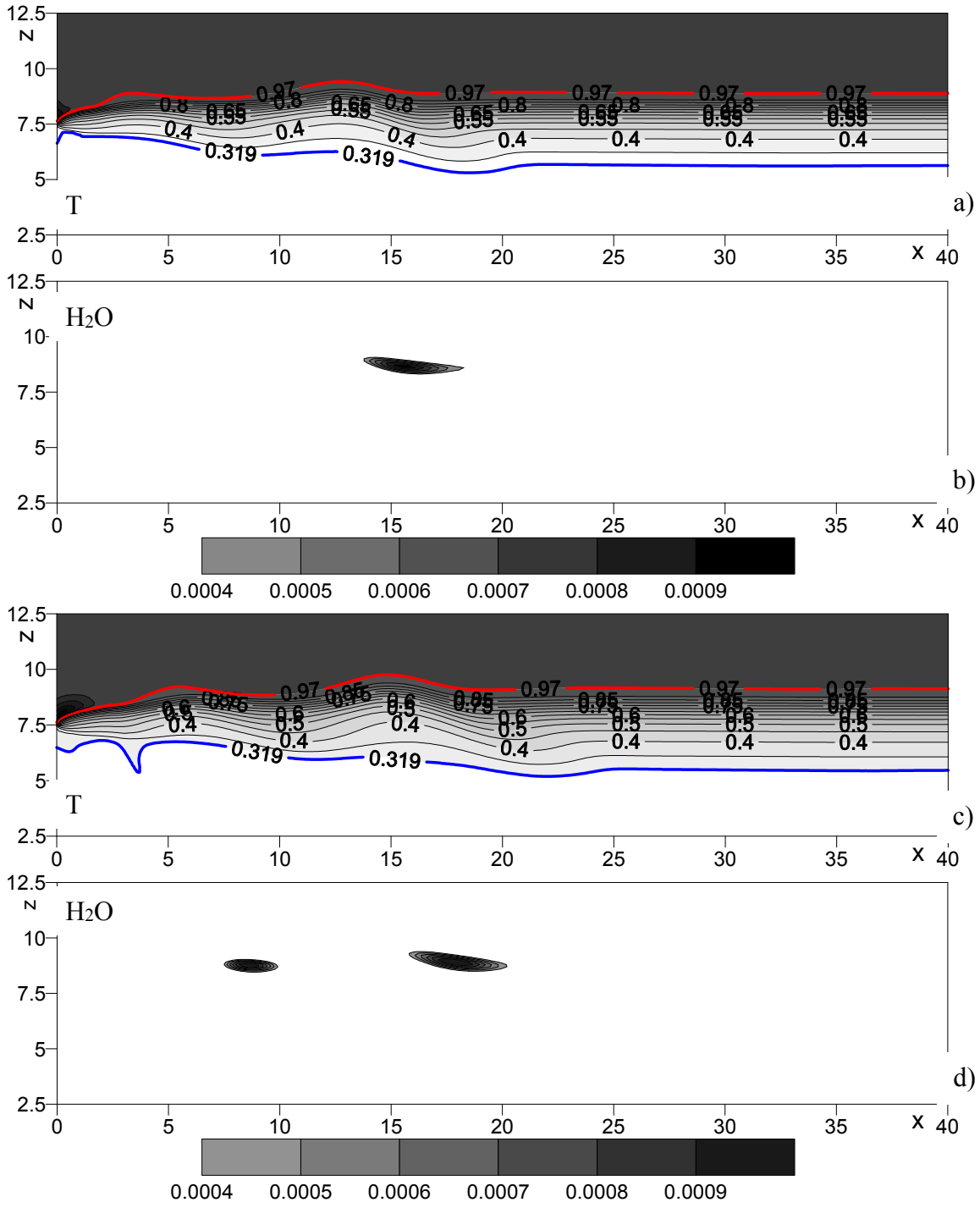

Figure 15 – The temperature field a, c) and formation of water vapor b, d) a-b) $M_0 = 1.1$, $M_\infty = 1.5$, c-d) $M_0 = 1.4$, $M_\infty = 1.8$

Conclusion

The flowfield structures of supersonic turbulent planar shear layer and combustion computed by calculation of the system of two-dimensional planar Favre-averaged Navier-Stokes equations. The k-ε two-equation turbulence model with compressibility correction is used to determine the eddy viscosity coefficient. The numerical method is based on the third order ENO finite-difference scheme. The

comparison of present results obtained by using ENO scheme and k-ε turbulence model with experimental data demonstrates a satisfactory prediction of mean and turbulence properties of the flow. The numerical results of hydrogen-air mixture combustion based on Jachimowski's seven-species seven reaction model.

The calculation reacting shear layer revealed distribution and enhancement of hydrogen-air mixing and combustion is strongly depend on vortices formation, a namely their intensity and growing. The present numerical experiments show that the combustion zone is concentrated in the upper (oxidizer) boundary of mixing layer.

It have been graphically illustrated that for the lower Mach numbers case the hydrogen-air mixture ignition is occurred faster than for the higher one.

Thus the constructed algorithm based on the high order scheme and computer code for turbulent supersonic reacting flow allows to study influence parameters that control mixing and combustion, which is important in the design of supersonic combustion ramjet (scramjet) engines and easily expanded into 3D case.

References

1. Winant C.D., Browand F.K. "Vortex pairing: the mechanism of turbulent mixing-layer growth at moderate Reynolds number." *J. Fluid Mech*. 63 (1974): 237-255.

2. Brown G.L., Roshko A. "On the density effects and large structures in turbulent mixing layers." *J. Fluid Mech.* 64 (1974): 775-816.

3. Bogdanoff D.W. "Compressibility effects in turbulent shear layers." *AIAA J.* 21 (1983.): 926-927.

4. Papamoschou D., Roshko A. "The compressible turbulent shear layer: an experimental study." *J. Fluid Mech*. 197 (1988): 453-477.

5. Chinzei N., Masuya G., Komuro T., Murakami A., Kudou K. "Spreading of two-stream supersonic turbulent mixing layers." *Phys. Fluids* 29 (1986): 1345-1347.

6. Goebel S. G., Dutton J.C. "Experimental study of compressible turbulent mixing layers." *AIAA J.* 29, no. 4 (1991): 538-546.

7. Oster D., Wygnanski I. "The forced mixing layer between parallel streams". *J. Fluid Mech.* 123 (1982): 91-130.

8. Samimy M., Elliot G.S. "Effects of compressibility on the characteristics of free shear layers." *AIAA J.* 28 (1990): 439-445.

9. Elliot G.S., Samimy M. "Compressibility effects in free shear layers." *Phys. Fluids A 2* (1990): 1231-1240.

10. Ju Y., Niioka T. "Ignition Analysis of Unpremixed Reactants with Chain Mechanism in a Supersonic Mixing Layer." *AIAA J.* 31, no. 5 (1993): 863-868.

11. Im H. G., Chao B. H., Bechtold J. K., Law C. K. "Analysis of Thermal Ignition in the Supersonic Mixing Layer." *AIAA J.* 32, no. 2 (1994): 341-349.

12. Cheng T.S., Lee K.S. "Numerical simulations of underexpanded supersonic jet and free shear layer using WENO schemes." *International Journal of Heat and Fluid Flow* 26 (2005): 755-770.

13. Tang W., Komerath N.M., Sankar L.N. "Numerical simulation of the Growth of instabilities in Supersonic Free Shear Layers." *J. Propulsion* 6, no. 4 (1990): 455-460.

14. Tang W., Sankar, L.N., Komerath, N. "Mixing enhancement in supersonic free shear layers." AIAA 2nd Shear Flow Conference, *AIAA J.* (1989): 89-98.

15. Reichert R.S., Biringen S. "Numerical simulation of compressible plane jets." *Mechanics Research Communications* 34 (2007): 249-259.

16. Dale A. Hudson *Numerical simulation of a confined supersonic shear layer*. PhD dissertation, (1996): 1-181.

17. Xiao-Tian Shi, Jun Chen, Wei-Tao Bi, Chi-Wang Shu, Zhen-Su She. "Numerical simulations of compressible mixing layers with a discontinuous Galerkin method." *Acta Mech. Sin.* 27, no.3 (2011): 318-329.

18. Zambon A.C., Sriram A.T., Chelliah H.K. "Development and Implementation of Explicit Reduced Reaction Models in Supersonic Reacting Shear Flow Simulations." 45th AIAA Aerospace Sciences Meeting and Exhibit, Reno, Nevada, *AIAA-2007* (2007): 772.

19. Sriram A.T., Zambon A.C., Chelliah H.K. "Validation of Ethylene-Air Reduced Reaction Models in Supersonic Shear Flows." 46th AIAA Aerospace Sciences Meeting and Exhibit, Reno, Nevada, *AIAA-2008* (2008): 993.

20. Da Silva L. F. F., Deshaies B., Champion M. "Some Specific Aspects of Combustion in Supersonic H2-Air Laminar Mixing Layers." *Combustion Science and Technology 89* (1993): 317-333.

21. Nishioka M., Law C.K. "A Numerical Study of Ignition in the Supersonic Hydrogen/Air Laminar

Mixing Layer." *Combustion and Flame* 108 (1997): 199-219.

22. Fang X., Liu F., Sirignano W. A. "Ignition and Flame Studies for an Accelerating Transonic Mixing Layer." *Journal of Propulsion and Power* 17, no. 5 (2001): 1058-1066.

23. Ju Y., Niioka T. "Reduced Kinetic Mechanism of Ignition for Nonpremixed Hydrogen/Air in a Supersonic Mixing Layer." *Combustion and Flame* 99 (1994): 240-246.

24. Ju Y., Niioka T. "Ignition Simulation of Methane/Hydrogen Mixtures in a Supersonic Mixing Layers." *Combustion and Flame* 102 (1995): 462-470.

25. Tahsini, A.M. "Ignition Analysis in Supersonic Turbulent Mixing Layer." *World Academy of Science, Engineering and Technology* 57 (2011): 353-357.

26. Tahsini A.M. "Ignition Time Delay in Swirling Supersonic Flow Combustion." *World Academy of Science, Engineering and Technology* 70 (2012): 623-627.

27. Chakraboty D., Paul P. J., Mukunda H. S. "Evaluation of Combustion Models for High Speed H2/Air Confined Mixing Layer Using DNS Data." *Combustion and Flame* 121 (2000): 195-209.

28. Kee R. J., Rupley F. M., Miller J. A. "CHEMKIN-II: a Fortran chemical kinetic package for the analysis of gas-phase chemical kinetics." *SANDIA Report SAND89-8009* (1989).

29. Poinsot T.J., Lele S.K. "Boundary conditions for direct simulation of compressible viscous flows." *Journal of Computational Physics* no. 101 (1992): 104-129.

30. Harten A., Osher S., Engquist B., Chakravarthy S.R. "Some Results on Uniformly High-Order Accurate Essentially Non-oscillatory Schemes." *Applied Num. Math*. 2 (1986): 347-377.

31. Yang J. Y. "Third order nonoscillatory schemes for the Euler equations." *AIAA J.* 29, no. 10 (1991): 1611-1618.

32. Bruel P., Naimanova A. Zh. "Computation of the normal injection of a hydrogen jet into a supersonic air flow." *Thermophysics and Aeromechanics* 17, no. 4 (2010): 531-542.

33. Belyayev Ye., Naimanova A. Zh.. "Two-Dimensional Supersonic Flow with Perpendicular Injection of the Gas." *Chapter 2 InTech open access book Advanced Methods for Practical Applications in Fluid Mechanics* (2012): 23-44.

34. Shuen J. Sh., Yoon S. "Numerical study of chemical reacting flows using a lower-upper symmetric successive overrelaxation scheme." *AIAA J.* 27, no. 12 (1989): 1752-1760.

35. Belyayev Ye., Kaltayev A., Naimanova A. Zh. "Supersonic Flow with Perpendicular Injection of a Hydrogen." Proceedings of 2010 2nd International Conference on Computer Engineering and Technology, *Mechanical and Aerospace Engineering* 5(2010): 531-534.

36. Cao D.G., He G.Q., Qin F., Wei X.G., Shi L., Liu B., Huang ZW. "LES study on flow features of the supersonic mixing layer affected by shock waves." *International communications in heat and mass transfer* 85 (2017): 114-123.